Experimental and Theoretical Investigation on Binary Semiconductor Clusters of Bi/Si, Bi/Ge, and Bi/Sn

Shutao Sun, Hongtao Liu, and Zichao Tang*

State Key Laboratory of Molecular Reaction Dynamics, Center of Molecular Science, Institute of Chemistry, Chinese Academy of Sciences, Beijing 100080, P.R. China

Received: December 12, 2005; In Final Form: February 3, 2006

$Bi_mM_n^-$ (M = Si, Ge, Sn) binary cluster anions are generated by using laser ablation on mixtures of Bi and M (M = Si, Ge, Sn) samples and studied by reflectron time-of-flight mass spectrometer (RTOF-MS) in the gas phase. Some magic number clusters are present in the mass spectra which indicate that they are in stable structures. For small anions ($m + n \leq 6$), their structures are investigated with the DFT method and the energetically lowest lying structures are obtained. For the binary anionic clusters with the same composition containing Si, Ge, and Sn, they share similar geometric and electronic structure in the small size except that $BiSi_3^-$, $BiSi_5^-$, $Bi_2Si_2^-$, $Bi_2Si_3^-$, and $Bi_4Sn_2^-$ are different for the lowest energetic structures, and the ground states for all the anions are in their lowest spin states. The calculated VDE (vertical detachment energy) and binding energy confirm the obviously magic number cluster of BiM_4^- (M = Si, Ge, Sn), which agrees with the experimental results.

1. Introduction

Structural and electronic property transitions of semiconductor clusters have been extensively studied in the past few decades for both fundamental and technological interests. Properties between semiconductor clusters and their bulk material are greatly different, and properties of clusters show strong and nonmonotonic variations with the increasing of the size, which provide potential for applications. As important semiconductor materials, group IV elemental clusters have attracted enormous experimental and theoretical studies. It has been shown that the structures are similar for Si_n, Ge_n, and Sn_n clusters for $n \leq 7$,[1−7] while the medium-sized clusters follow the different growth pattern and there are still present some controversial results.[8−15] Many experimental data for the neutral semiconductor clusters were obtained from experiments on the anionic clusters. Smalley and co-workers performed photoelectron spectroscopy (PES) experiments on the Si_n^-, Ge_n^- ($3 \leq n \leq 12$).[16] Neumark's group has done photoelectron and zero electron kinetic energy spectroscopic (ZEKE) studies on Ge_n^- ($n = 2-15$).[17] The photoelectron spectra observed for Sn_n^- were similar to those of Si_n^-, Ge_n^-.[18,19] And Kaya et al. estimated the HOMO-LUMO gap of Si_n, Ge_n, Sn_n clusters using PES of their halogen-doped anionic clusters.[20] Theoretical investigations on anions of these semiconductor clusters suggest that upon charging the neutral clusters negatively, the ground state structure may significantly change in comparison to the neutral cases.[21−24]

Bismuth, the heaviest group V semimetal element, was among the first materials that seemed to be interesting for thermoelectric application and its properties have been investigated in detail in the 60's.[25] Nowadays bismuth nanoparticles have also been attracting extensive studies as an interesting material for electronics because of their highly anisotropic electronic behavior, low conduction band, high electron mobility, and potential for inducting a semiconductor transition with decreasing crystallite size.[26−31] When doped with other substances, in particular with elements in group IV, a profound effect has been shown on the transport properties of bismuth, and many studies have been preformed on Si, Ge, Sn-doped Bi,[32−35] and Bi adsorption on Si, Ge, Sn surfaces.[36−39] In the gas phase, Meloni et al. investigated the atomization energies and enthalpies of formation of $SnBi_n$ ($n = 1-3$) gaseous molecules by Knudsen cell mass spectrometry.[40] But there are few studies on the binary clusters consisted of Si, Ge, Sn with Bi.

Cluster is an intermediate phase between single atom and bulk materials. A fundamental pursuit of cluster science is to understand how the geometric and electronic structures of clusters change with its aggregation size increasing from single atom to bulk materials. With the continuous trend of current day's miniaturization, minimum electronic devices will soon approach the size of atomic clusters, and the stable clusters may be used as the building blocks for cluster-assembled materials. In this work, a series of binary alloy anionic clusters $Bi_mSi_n^-$, $Bi_mGe_n^-$, and $Bi_mSn_n^-$ produced by laser ablation are studied both experimentally with RTOF-MS and theoretically with the results using DFT.

2. Experimental Method

The apparatus consists of a Smalley-type[41] laser vaporization source and a homemade high-resolution reflectron time-of-flight mass spectrometer (similar to that of Mamyrin[42]). A detailed description of the apparatus has been given elsewhere.[43]

The binary samples were prepared with Bi (purity >99.9%) and M (M = Si, Ge, Sn; Si purity >99%; Ge, Sn purity >99.9%) powders, mixed well in atomic ratios (1:1), and pressed into sample disks. Then the sample targets were ablated by the focused second harmonic output of a Nd:YAG laser (10 mJ/pulse, 10 Hz, 1 mm in diameter beam spot) and the targets were rotated in the experiment process. The sample particles were vaporized into the tube reactors (3×10 mm^2) and entrained with the carrier gas argon with the backing pressure of about 4 atm, then the beam underwent a supersonic

* Address correspondence to this author. E-mail: zctang@iccas.ac.cn.

10.1021/jp057242b CCC: $33.50
Published on Web 03/29/2006

expansion. After passing a skimmer, the beam entered the accelerator region in the RTOF-MS. The products were then extracted perpendicularly by the pulsed electric field and accelerated to about 1.2 keV. They experienced two sets of deflectors and einzel electrostatic lenses and then were reflected by a reflector. Finally the ions reached the space focus, where a dual microchannel plate (MCP) was installed. The output signal was amplified and recorded by a 100 MHz transient recorder (USTC, China), then was stored by a PC computer. The timing of the valve opening, laser vaporization, pulse acceleration, and recording was optimized in a digital delay pulse generator (Stanford Research DG535). Typically the final digitized mass spectra were averaged 300 laser pulses and the mass resolution of the mass spectrometer ($m/\Delta m$) is over 1000 under the present conditions.

The source chamber, the flight tube, and the reflectron region were all differentially pumped with turbomolecular pumps and mechanical pumps. The corresponding operating pressures were 10^{-4}, 10^{-6}, and 10^{-7} Torr, respectively.

3. Theoretical Method

In this work, geometric and electronic structure calculations on these binary clusters have been performed by using B3LYP and B3PW91 functionals, which are two widely used hybrid DFT-HF methods.

Two types of basis sets were used in both geometry and frequency calculations. In the first type of basis set, the relativistic effective core potentials (RECPs) given by Hay/Wadt[44] and the corresponding LANL2DZ basis sets were used for all the elements, and the LANL2DZ basis sets were extended by an additional set of diffuse and polarization functions[45] appropriate for studying anions in this study. RECPs are common and efficient ways to reduce the complex calculations for molecules containing heavy atoms such as Sn and Bi, which replace the chemically inert core electrons with potentials and incorporate relativistic effects in the potentials.

For the elements Si and Ge, we used the all-electron basis set 6-311+g(3df) in the second type of basis sets to compare the results. Whereas there are no standard 6-311+g(3df) for elements Sn and Bi, the above RECPs basis sets were still used. For the sake of brevity, the first type of basis sets is referred to as LANL2DZdp and the second is labeled as 6-311+g(3df) in the present paper. The theoretical method and basis sets have been successfully applied to systems containing Sn and Pb,[46,47] so should be adequate for studying on Bi-containing clusters.

To search for the global minima of $Bi_mM_n^-$ (M = Si, Ge, Sn), we have first performed first-principles DFT calculations on a wide variety of singlet and triplet structures (or doublet and quadruplet) for these species at the level of B3LYP/LANL2DZdp and B3PW91/LANL2DZdp. To characterize the nature of the stationary points, harmonic vibrational frequencies were calculated. The calculated results agree well with those of these two methods. We found that the most stable structures for all these anionic species are present as their lowest spin (singlet or doublet) electronic state. Then we further examined the geometries and calculated the frequencies at B3LYP/6-311+g(3df) and B3PW91/6-311+g(3df) levels. The optimized geometries, vibrational frequencies, and relative energies are consistent with the results by LANL2DZdp basis sets. All the calculations were carried out with the Gaussian 98 program package.[48]

4. Results and Discussion

4.1. Product Analysis with the Mass Spectrometer. Figure 1a−c shows the mass spectra of the cluster anions resulting from laser ablation on the samples Bi/Si, Bi/Ge, and Bi/Sn, respectively. The high resolution of our RTOF-MS allows the exact identification of the isotopic distribution in the mass region of these spectra. In these experiments, cluster-sized "magic numbers" are observed.

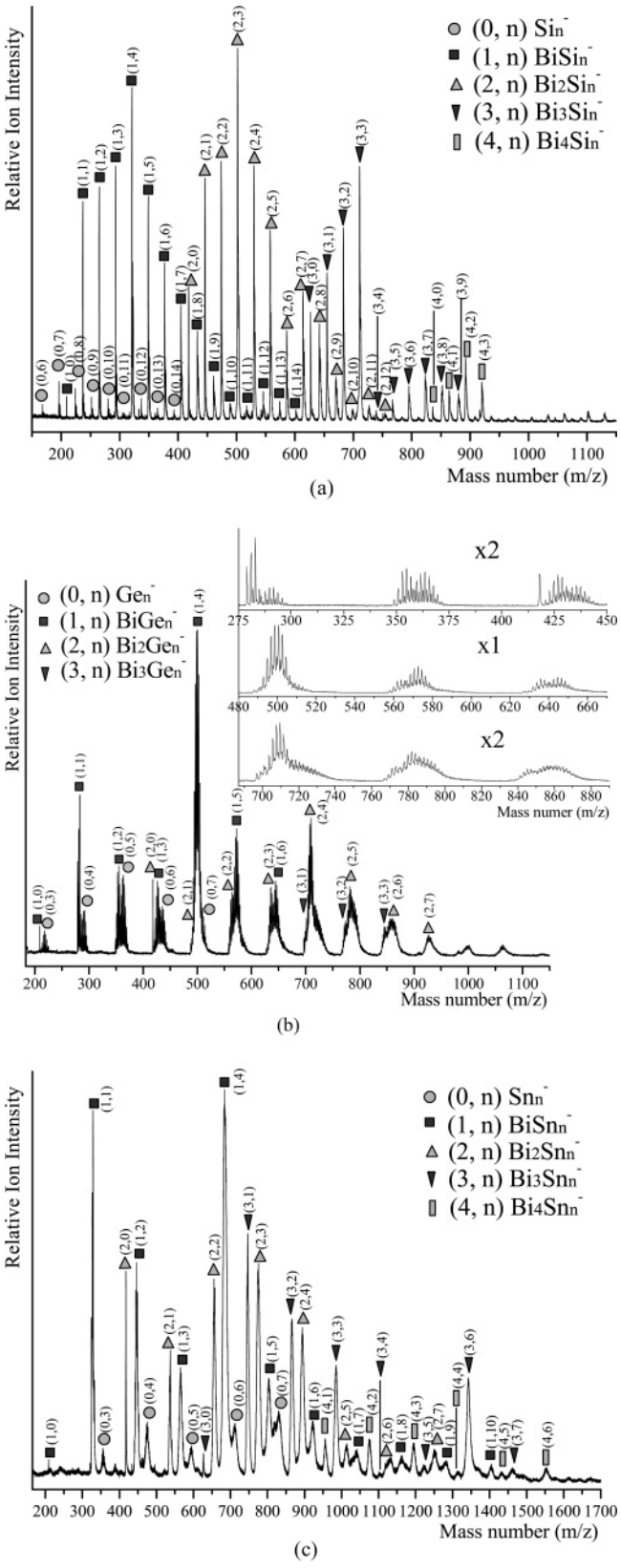

Figure 1. TOF mass spectra of binary cluster anions produced by laser ablation on mixed samples of (a) Bi/Si (atomic ratio 1:1), (b) Bi/Ge (atomic ratio 1:1), and (c) Bi/Sn (atomic ratio 1:1).

From Figure 1a, we can see five different series of products for $Bi_mSi_n^-$. In the $BiSi_n^-$ series (n is assigned clearly from 0 to 14), the $BiSi_4^-$ is the magic number species due to its larger intensity than the others, which suggests that it is a very stable structure. And the increasing signal of $BiSi_{12}^-$ hints that it is in a relatively stable structure compared with its neighboring clusters in the same series. The series in the lower mass region are the homoatomic Si_n^- clusters that we will not discuss here. In the case of the $Bi_2Si_n^-$ ($n = 0-12$) series, the $Bi_2Si_3^-$ cluster shows much more intense peaks than the other ones close to it, and $Bi_2Si_6^-$ seems unstable compared with $Bi_2Si_7^-$. When the number of Si atom increases from 0 to 3, the intensity of $Bi_3Si_n^-$ clusters also increases in succession, but the relative intensity of $Bi_3Si_4^-$ drops suddenly leading to a very weak peak, then increases gradually from $n = 5$ up to $n = 7$ and decreases again from $n = 8$ to $n = 9$. So the magic number clusters in this series are $Bi_3Si_3^-$ and $Bi_3Si_7^-$. The signals for $Bi_4Si_n^-$ are small, and $Bi_4Si_2^-$ is the largest one in this series.

For the mass spectra of $Bi_mGe_n^-$ binary clusters, because the isotopic distributions for some products partly overlap each other due to the close mass numbers, we identify the peaks carefully by the isotope distributions and the relative intensities. The pure negative charged clusters Ge_3^- to Ge_7^- can be seen in the spectra. The peak for $BiGe^-$ is strong before the mass of the Ge_4^- cluster. The intensities of $BiGe_2^-$ and $BiGe_3^-$ are smaller than that of $BiGe^-$ and they occur just before the mass of Ge_5^-, Ge_6^-, respectively. The mass peaks for Bi_2Ge^- and $BiGe_4^-$ are a little overlapped, and $BiGe_4^-$ overlaps with Ge_7^- partly too, which can be seen clearly from the enlarged spectrum. As an example, we list the respective isotopic distributions of Bi_2Ge^- and $BiGe_4^-$ to elucidate these peaks more directly: Bi_2Ge^- (isotope mass, relative abundance: 487.9, 0.56; 489.9, 0.75; 490.9, 0.21; 491.9, 1.00; 493.9, 0.21) and $BiGe_4^-$ (isotope mass, relative abundance: 488.7, 0.01; 490.7, 0.06; 491.7, 0.02; 492.7, 0.20; 493.7, 0.07; 494.7, 0.46; 495.7, 0.18; 496.7, 0.78; 497.7, 0.31; 498.7, 1.00; 499.7, 0.38; 500.7, 0.99; 501.7, 0.33; 502.7, 0.73; 503.7, 0.20; 504.7, 0.40; 505.7, 0.07; 506.7, 0.15; 507.7, 0.01; 508.7, 0.03; 509.7, 0.001; 510.7, 0.004). Therefore we can make out that $BiGe_4^-$ is the strongest intensity cluster in the $BiGe_n^-$ ($n = 1-6$) series, just like the $BiSi_n^-$ series, while the intensities for Bi_2Ge^- and Ge_7^- are much weaker than that of $BiGe_4^-$. Likewise, the mass peaks for the following pairs $Bi_2Ge_2^-$ and $BiGe_5^-$; $Bi_2Ge_3^-$ and $BiGe_6^-$; Bi_3Ge^- and $Bi_2Ge_4^-$; $Bi_3Ge_2^-$ and $Bi_2Ge_5^-$; and $Bi_3Ge_3^-$ and $Bi_2Ge_6^-$ are a little overlapped, respectively, but their relative intensities are not hard to compare. In the series of $Bi_2Ge_n^-$ mass peaks, the intensity for $Bi_2Ge_4^-$ is presented largest in the spectra. $Bi_3Ge_n^-$ ($n = 1-3$) is a weak series in the mass spectra.

The mass spectra for $Bi_mSn_n^-$ clusters are shown in Figure 1c. We can figure out the mass and intensity for each species clearly because the mass of these clusters is separated from each other in an obvious manner. $BiSn_n^-$ ($n = 0-10$) are present in the first series, $BiSn^-$ and $BiSn_4^-$ are the magic number species, just like $BiGe_n^-$; they are the sharp turning point in the spectra. The intensity of $Bi_2Sn_3^-$ is the largest one among the mass peaks of $Bi_2Sn_n^-$ ($n = 0-7$), and the peak of $Bi_2Sn_7^-$ is larger than that of $Bi_2Sn_6^-$, the same as the $Bi_2Si_n^-$ clusters. As to the series of $Bi_3Sn_n^-$ ($n = 0-7$), the turning point occurs at the mass positions of Bi_3Sn^- and $Bi_3Sn_6^-$. $Bi_4Sn_n^-$ ($n = 1-6$) show weak mass peaks in our spectra.

From the above analysis, we can see that in the mass range of this work, there exit large similarities for the cluster anions resulting from the Bi/Si, Bi/Ge, and Bi/Sn samples.

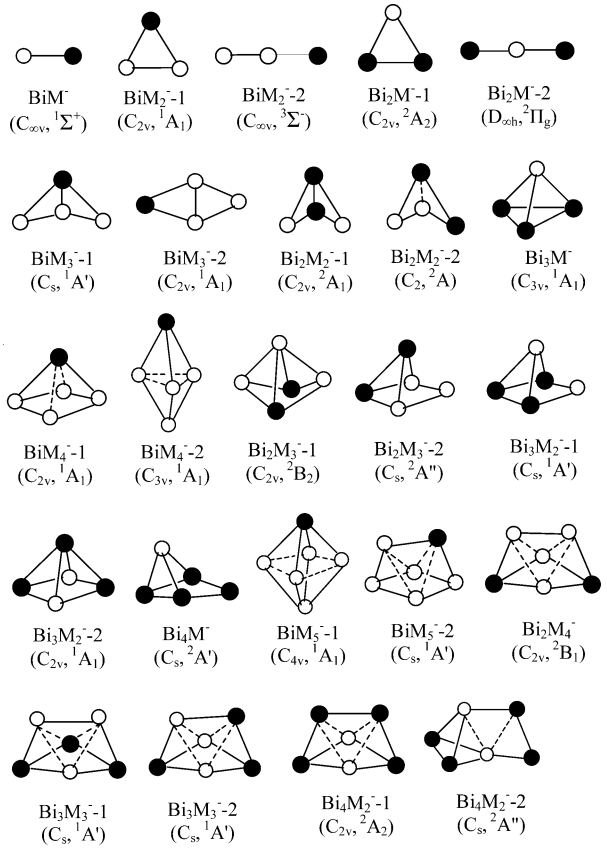

Figure 2. Optimized lowest energy structures for $Bi_mM_n^-$ (M = Si, Ge, Sn; $m + n \leq 6$). Open circles represent M atoms and the solid ones stand for Bi atoms.

4.2. Structure by the DFT Calculation. We have optimized a number of various initial structures with the different spin states, and the normal vibrational frequencies at the optimized geometries are also checked for imaginary frequencies at the same theoretical level. The optimized lowest lying energy structures for these species are depicted in Figure 2. For all these anions, the lowest spin state is lower in energy than the higher spin state in their respectively optimized structure. As the cluster size increases, it becomes much more difficult to find the lowest energy structure in theoretical studies because the number of possible geometries increases exponentially. Moreover, because the larger size $Bi_mGe_n^-$ clusters are not obtained in this experiment, we have just calculated the structures for the anionic clusters in the size of $m + n \leq 6$.

4.2.1. Linear BiM^- (M = Si, Ge, Sn). All BiM^- binary anions $BiSi^-$, $BiGe^-$, and $BiSn^-$ have singlet ground states ($C_{\infty v}$, $^1\Sigma^+$) with the LANL2DZdp basis set or the 6-311+G(3df) basis set from B3LYP and B3PW91 methods. The two hybrid DFT functionals yield similar geometries and B3LYP with a tendency for slightly longer bonds than B3PW91. In the following, unless indicated otherwise, the geometries discussed refer to the B3LYP calculations only. The shortest distances between two atoms in the crystals of Si, Ge, Sn, and Bi are about 2.35, 2.45, 3.02, and 3.11 Å from the XRD (X-ray diffraction) experiment. For the bond lengths of binary anions $BiSi^-$ and $BiGe^-$, we obtained 2.391, 2.479 Å with the 6-311+G(3df) basis set, respectively. And the calculated bond distance of the anionic $BiSn^-$ is 2.650 and 2.642 Å at B3LYP/LANL2DZdp and B3PW91/LANL2DZdp levels, respectively.

4.2.2. Triangular BiM_2^- and Bi_2M^- (M = Si, Ge, Sn). In the case of clusters composed of three elements, the ground states for all BiM_2^- and Bi_2M^- are $^1A_1$ and $^2A_2$, respectively, both in

C_{2v} triangular structures. For $BiSi_2^-$ and $BiGe_2^-$, the excited state $C_{\infty v}$ ($^3\Sigma^-$) linear structures lie only 0.76, 0.83 eV higher in energy than their ground states, and the bond between Si−Si appears to be a double bond (2.193 Å). The optimizations of $BiSn_2^-$ and Bi_2Sn^- at the B3LYP/LANL2DZdp level reveal that their ground states are also $^1A_1$ and $^2A_2$ C_{2v} triangular structures, with the excited-state $C_{\infty v}$ ($^3\Sigma^-$) linear structure as a low-lying state for $BiSn_2^-$. The other two linear ($D_{\infty h}$, $C_{\infty v}$) isomeric structures with singlet states, which are not shown in Figure 2, are calculated to compare with the triangular structure. The energies for $BiSi_2^-$, $BiGe_2^-$, Bi_2Si^-, and Bi_2Ge^- in the $C_{\infty v}$ isomers at the B3LYP/6-311+G(3df) level are 1.36, 1.42, 1.44, and 1.40 eV higher than those of the C_{2v} structure, and the isomers in this $D_{\infty h}$ symmetry of $BiSi_2^-$, $BiGe_2^-$, Bi_2Si^-, and Bi_2Ge^- are 2.28, 2.00, 0.46, and 0.63 eV higher than those of the ground state.

4.2.3. BiM_3^-, $Bi_2M_2^-$, and Bi_3M^- (M = Si, Ge, Sn). $BiSi_3^-$ has a $^1A_1$ ground state of planar C_{2v} symmetry, with a low-lying, nearly degenerate, $^1A'$ state of C_s symmetry with a butterfly structure, which is located 0.02 eV above the $^1A_1$ ground state, while in the case of $BiGe_3^-$ and $BiSn_3^-$, the $^1A'$ state of C_s symmetry is predicted to be the ground state, more stable by about 0.28, 0.45 eV than their respectively planar C_{2v} structures. As for the $Bi_2M_2^-$ anionic clusters, the $^2A_1$ (C_{2v}) state with butterfly structures is the ground state for $Bi_2Ge_2^-$ and $Bi_2Sn_2^-$, but the ^2A (C_2) state is the ground state for $Bi_2Si_2^-$, appearing to be more stable by 0.11 eV than the C_{2v} symmetry isomer. Frequency analysis indicates that another isomer with the D_{2h} planar rhombus structure is a first-order stationary point for $Bi_2Si_2^-$, $Bi_2Ge_2^-$, and $Bi_2Sn_2^-$. As to the Bi_3M^- clusters, the calculation results indicate that they all take the singlet state ($^1A_1$) of C_{3v} trigonal pyramid structure as the ground state, with bond lengths of 2.756, 2.818, 3.100 Å for the Bi−Si, Bi−Ge, and Bi−Sn bonds, and the bond length for Bi−Bi is similar. The energies of the other isomers, C_s butterfly or planar C_{2v} structures, are much higher than those of their ground states.

4.2.4. BiM_4^-, $Bi_2M_3^-$, $Bi_3M_2^-$, and Bi_4M^- (M = Si, Ge, Sn). For $Bi_mM_n^-$ with $m + n \geq 5$, the clusters have several possible isomers with little difference in structures and energies. We present here the energetically lowest lying structures, which are the most likely candidates for the ground states of the corresponding anionic clusters. For BiM_4^-, the singlet state ($^1A_1$) of the C_{2v} distorted trigonal bipyramidal isomer is the most stable structure. Another trigonal bipyramidal (C_{3v}) structure for $BiSi_4^-$, $BiGe_4^-$, and $BiSn_4^-$ is 0.34, 0.19, and 0.13 eV above their ground states, respectively. As to $Bi_2M_3^-$, the energy of the C_s ($^2A''$) structure is very close to that of the C_{2v} ($^2B_2$) structure. The C_{2v} distorted trigonal bipyramidal structure is found to be 0.09 eV higher in energy than the C_s structure for $Bi_2Si_3^-$, whereas the energy is 0.03 and 0.14 eV lower for $Bi_2Ge_3^-$ and $Bi_2Sn_3^-$, respectively. $Bi_3Si_2^-$, $Bi_3Ge_2^-$, and $Bi_3Sn_2^-$ prefer a C_s ($^1A'$) symmetry structure, more stable than another C_{2v} ($^1A_1$) low-lying energetic structure by 0.13, 0.13, and 0.09 eV respectively. For Bi_4M^-, the ground states are all a C_s symmetry structure with a $^2A'$ electronic state.

4.2.5. BiM_5^-, $Bi_2M_4^-$, $Bi_3M_3^-$, and $Bi_4M_2^-$ (M = Si, Ge, Sn). $BiGe_5^-$ and $BiSn_5^-$ have the high C_{4v} symmetry of the tetragonal bipyramidal structure ($^1A_1$) as their ground states, with a low-lying bicapped tetrahedron structure of C_s symmetry 0.16 and 0.34 eV higher in energy, respectively, whereas the case is reverse for $BiSi_5^-$, with the C_s symmetry ($^1A'$) 0.07 eV more stable than the C_{4v} structure. For $Bi_2M_4^-$, the ground states are all the doublet states ($^2B_1$) with a C_{2v} bicapped tetrahedron structure in which Bi atoms are the two capped atoms. $Bi_3Si_3^-$ and $Bi_3Ge_3^-$ have a C_s ($^1A'$) ground state of a bicapped tetrahedron structure, and another low-lying C_s symmetry bicapped tetrahedron structure lying 0.35 and 0.13 eV above in energy at the B3LYP/6-311+G(3df) level, respectively. For $Bi_3Sn_3^-$, these two structures are lowest in energy, nearly degenerate, and both are likely candidates for the ground state at the B3LYP/LANL2DZdp level. Likewise, $Bi_4Si_2^-$ and $Bi_4Ge_2^-$ have a C_s ($^2A''$) ground-state structure, as well as a low-lying energetic structure of C_{2v} symmetry that is 0.66 and 0.21 eV higher in energy. While the reverse is the case for $Bi_4Sn_2^-$, it presents the C_{2v} ($^2A_2$) structure as the lowest energetic isomer, which is 0.16 eV more stable than the C_s symmetry isomer.

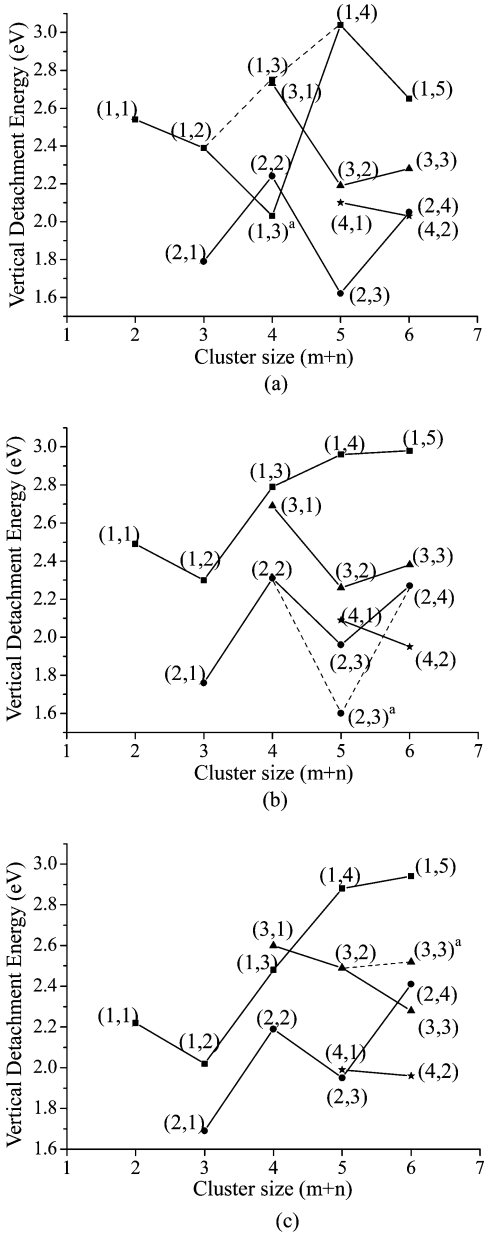

Figure 3. Vertical detachment energies of $Bi_mM_n^-$ (M = Si, Ge, Sn; $m + n \leq 6$) (a) $Bi_mSi_n^-$, (b) $Bi_mGe_n^-$, and (c) $Bi_mSn_n^-$ by the B3LYP method. The superscript "a" indicates the nearly degenerate isomer.

4.3. Vertical Detachment Energy. The VDE corresponds to transitions from the ground electronic states of the anion to the ground electronic state of the neutral molecule with identical anionic geometry. We have calculated VDE with B3LYP and B3PW91 methods corresponding to their respective optimized structures, and the results are in good agreement. The VDE

TABLE 1: Binding Energies (BE, in eV/atom), Energy Gain (Δ, in eV), and the Second-Order Energy Difference (ΔE^n, in eV) of $Bi_mM_n^-$ (M = Si, Ge, Sn; $m + n \leq 6$) Clusters by the B3LYP Method

	$BiSi^-$	$BiSi_2^-$	$BiSi_3^-$	$BiSi_4^-$	$BiSi_5^-$	Bi_2Si^-	$Bi_2Si_2^-$	$Bi_2Si_3^-$	$Bi_2Si_4^-$	Bi_3Si^-	$Bi_3Si_2^-$	$Bi_3Si_3^-$	Bi_4Si^-	$Bi_4Si_2^-$
BE	2.56	2.82	3.00	3.30	3.22	2.41	2.67	2.85	2.92	2.52	2.60	2.67	2.30	2.45
Δ		3.33	3.55	4.49	2.85		3.47	3.57	3.27		2.92	3.02		3.22
ΔE^n		−0.218	−0.941	1.643			−0.112	0.310			−0.112			
	$BiGe^-$	$BiGe_2^-$	$BiGe_3^-$	$BiGe_4^-$	$BiGe_5^-$	Bi_2Ge^-	$Bi_2Ge_2^-$	$Bi_2Ge_3^-$	$Bi_2Ge_4^-$	Bi_3Ge^-	$Bi_3Ge_2^-$	$Bi_3Ge_3^-$	Bi_4Ge^-	$Bi_4Ge_2^-$
BE	2.49	2.67	2.82	3.05	2.99	2.36	2.57	2.70	2.76	2.49	2.54	2.58	2.27	2.35
Δ		3.04	3.25	3.97	2.67		3.22	3.22	3.05		2.76	2.78		2.75
ΔE^n		−0.218	−0.713	1.292			0.003	0.163			−0.005			
	$BiSn^-$	$BiSn_2^-$	$BiSn_3^-$	$BiSn_4^-$	$BiSn_5^-$	Bi_2Sn^-	$Bi_2Sn_2^-$	$Bi_2Sn_3^-$	$Bi_2Sn_4^-$	Bi_3Sn^-	$Bi_3Sn_2^-$	$Bi_3Sn_3^-$	Bi_4Sn^-	$Bi_4Sn_2^-$
BE	2.18	2.32	2.42	2.59	2.56	2.18	2.35	2.42	2.44	2.36	2.37	2.37	2.18	2.21
Δ		2.60	2.72	3.29	2.38		2.86	2.68	2.54		2.40	2.37		2.38
ΔE^n		−0.117	−0.571	0.912			0.182	0.136			0.014			

values for the lowest energy anion structures calculated by B3LYP functional are present versus cluster size ($m + n \leq 6$) in Figure 3a−c. Up to now, there has been no available experimental value of VDE for these clusters to assist in the assignment for their structures. The calculated VDEs in the present size range exhibit an obvious turning point and maxima around BiM_4^- in agreement with the magic number clusters BiM_4^- (M = Si, Ge, Sn) observed in the time-of-flight mass spectra.

4.4. Binding Energy. Table 1 shows the binding energy per atom for the lowest energy structure for $Bi_mM_n^-$ (M = Si, Ge, Sn; $m + n \leq 6$) in each size. The binding energy (BE) is defined as follows: $BE = -[E(Bi_mM_n^-) - mE(Bi) - nE(M)]$. It is found that the BE/atom (binding energies divided by the total number of atoms in the cluster) is the largest for BiM_4^- in all these clusters. And for BiM_4^- clusters, the energy gain, $\Delta = -[E(Bi_mM_n^-) - E(Bi_mM_{n-1}^-) - E(M)]$, is also higher than that of the other clusters. Moreover, the second-order difference in energy is also calculated, $\Delta E^n = E(Bi_mM_{n+1}^-) + E(Bi_mM_{n-1}^-) - 2E(Bi_mM_n^-)$, and the value is also the largest one for BiM_4^-. Therefore, the BiM_4^- (M = Si, Ge, Sn) anions are indeed the magic number clusters in the $Bi_mM_n^-$ species. The relative high intensity for $Bi_3Si_3^-$ can also be explained by the calculated BE and energy gain (Δ).

4.5. HOMO-LUMO Gap of Bi_2M_n (M = Si, Ge, Sn). In the mass spectra, besides BiM_4^-, the mass signals for $Bi_2Si_3^-$, $Bi_2Ge_4^-$, and $Bi_2Sn_3^-$ are somewhat stronger than those of other clusters in their same series. Therefore, we calculated the HOMO-LUMO energy gap for the closed-shell neutral Bi_2M_n (M = Si, Ge, Sn; $n = 1-4$) species using B3LYP and B3PW91 methods at their respectively optimized lowest energy neutral structures (Figure 2S, Supporting Information). The calculated gaps for Bi_2M_n are somewhat larger than those of the pure semiconductor clusters, but similar to those of the DFT calculated HOMO-LUMO gaps for Si_mGe_n semiconductor binary clusters.[49] We note that the HOMO-LUMO gaps of Bi_2M_3 in Table 2 are considerably larger than their neighboring clusters. Much work has shown that clusters with large HOMO-LUMO gaps tend to be highly stable.[50−54] So we suggest that Bi_2M_3 are in relatively high stability and abundance among the neutral products. Furthermore, the structures for the anionic and neutral Bi_2M_3 are similar. Therefore, the high-intensity mass peaks of $Bi_2Si_3^-$ and $Bi_2Sn_3^-$ in the anion mass spectra are not difficult to understand, the abundance of neutral Bi_2M_3 gives them more opportunities thus allowing them to form anions more easily by combining an electron in the plasma. And the relative intensities for the anionic $Bi_2M_3^-$ and $Bi_2M_4^-$ clusters are affected by the combined results of the following factors: the quantities of the neutral species, VDE, and binding energies of the anions.

TABLE 2: HOMO-LUMO Gap of Neutral Clusters Bi_2M_n (M = Si, Ge, Sn; $n = 1-4$) Obtained from B3LYP and B3PW91, Respectively

			HOMO-LUMO gap (eV)	
	point group	state	B3LYP	B3PW91
Bi_2Si	C_{2v}	$^1A_1$	2.41	2.43
Bi_2Si_2	C_2	^1A	2.55	2.56
Bi_2Si_3-1	C_{2v}	$^1A_1$	3.32	3.35
Bi_2Si_3-2[a]	C_s	$^1A'$	3.04	3.10
Bi_2Si_4	C_{2v}	$^1A_1$	1.68	1.72
Bi_2Ge	C_{2v}	$^1A_1$	2.50	2.54
Bi_2Ge_2	C_{2v}	$^1A_1$	2.89	2.90
Bi_2Ge_3	C_{2v}	$^1A_1$	3.30	3.36
Bi_2Ge_4-1	D_{4h}	$^1A_{1g}$	2.91	2.91
Bi_2Ge_4-2[a]	C_{2v}	$^1A_1$	1.56	1.61
Bi_2Sn	C_{2v}	$^1A_1$	2.30	2.32
Bi_2Sn_2	C_{2v}	$^1A_1$	2.60	2.61
Bi_2Sn_3	C_{2v}	$^1A_1$	2.89	2.92
Bi_2Sn_4-1	D_{4h}	$^1A_{1g}$	2.80	2.81
Bi_2Sn_4-2[a]	C_{2v}	$^1A_1$	1.50	1.53

[a] The energetically low-lying neutral structures in similar symmetry with their corresponding anionic species. See Figure 2S.

4.6. Large Clusters. As to the larger clusters obtained in experiment without calculation results here, we compare them with the metal-doping semiconductor clusters. There is a lot of experimental[55−58] and theoretical investigation[51,59−62] on $TMSi_n$ (TM = transition metal) clusters, especially on $TMSi_{12}$ due to its high stability. Most of the $TMSi_{12}$ clusters are found to be hexagonal prisms with TM in the center. From the mass spectra, $BiSi_{12}^-$ is a stable structure, but unlike the transition metal, Bi is a semimetal of group V, which has no empty 5d orbitals, so its bonding with Si_{12} and the geometry of $BiSi_{12}^-$ has to be studied further. $Bi_3Si_7^-$ is also in relatively higher intensity compared with neighbors of the same series in our spectra, and its stability needs further calculation to be illuminated. $Bi_3Sn_6^-$ is a very stable species from our mass spectra, and its stability can be explained by the shell closing of the valence electrons (40) with the spherical cluster model, which maybe suggests the transition from the semiconductor to the metallic nature of the Bi_mSn_n cluster.

5. Conclusions

Bi/M (M = Si, Ge, Sn) binary cluster anions are produced and analyzed in the gas phase, and the most possible structures are obtained by DFT calculations. Full structural optimization and frequency analysis reveal that $Bi_mM_n^-$ (M = Si, Ge, Sn) follow similar structural patterns in the size range of $m + n \leq$

6, and the ground states of these anionic clusters are all low spin electronic states, which are consistent with the pure anionic semiconductor clusters. The calculated VDE and binding energy confirm the obviously magic number cluster of BiM_4^- in these anion species, which agrees well with the experimental results. And the theoretically large HOMO-LUMO gaps of the closed-shell neutral Bi_2M_3 clusters suggest their stabilities in the neutral products. The larger magic number clusters without calculation results need further theoretical confirmation.

Acknowledgment. The authors gratefully acknowledge the support of the National Natural Science Foundation of China under Grant Nos. 20203020 and 20433080. We thank Professor Qihe Zhu and Zhen Gao for their original design and assembly of the experimental apparatus.

Supporting Information Available: Figure 1Sa−c presents the detailed optimized lowest energy structures for $Bi_mM_n^-$ (M = Si, Ge, Sn; $m + n \leq 6$); Figure 2S shows the optimized lowest energy structures for neutral clusters Bi_2M_n (M = Si, Ge, Sn; $n = 1-4$). This material is available free of charge via the Internet at http://pubs.acs.org.

References and Notes

(1) (a) Raghavachari, K.; Logovinsky, V. *Phys. Rev. Lett.* **1985**, *55*, 2853. (b) Raghavachari, K.; Rohlfing, C. M. *J. Chem. Phys.* **1988**, *89*, 2219. (c) Rohlfing, C. M.; Raghavachari, K. *Chem. Phys. Lett.* **1990**, *167*, 559.
(2) Sankey, O. F.; Niklewski, D. J.; Drabold, D. A.; Dow, J. D. *Phys. Rev. B* **1990**, *41*, 12750.
(3) Binggeli, N.; Chelikowsky, J. R. *Phys. Rev. B* **1994**, *50*, 11764.
(4) Jackson, P.; Dance, I. G.; Fisher, K. J.; Willett, G. D.; Gadd, G. E. *Int. J. Mass Spectrom. Ion Processes* **1996**, *158*, 329.
(5) Lu, Z. Y.; Wang, C. Z.; Ho, K. M. *Phys. Rev. B* **2000**, *61*, 2329.
(6) Vasiliev, I.; Öğüt, S.; Chelikowsky, J. R. *Phys. Rev. Lett.* **1997**, *78*, 4805.
(7) Ballone, P.; Andreoni, W.; Car, R.; Parrinello, M. *Phys. Rev. Lett.* **1988**, *60*, 271.
(8) Ho, K. M.; Shvartsburg, A. A.; Pan, B.; Lu, Z. Y.; Wang, C. Z.; Wacher, J. G.; Fye, J. L.; Jarrold, M. F. *Nature* **1998**, *392*, 582.
(9) Shvartsburg, A. A.; Jarrold, M. F. *Phys. Rev. A* **1999**, *60*, 1235.
(10) Tai, Y.; Murakami, J. *J. Chem. Phys.* **2002**, *117*, 4317.
(11) Jarrold, M. F.; Constant, V. A. *Phys. Rev. Lett.* **1991**, *67*, 2994.
(12) Wang, J. L.; Wang, G. H.; Zhao, J. J. *Phys. Rev. B* **2001**, *64*, 205411.
(13) Majumder, C.; Kumar, V.; Mizuseki, H.; Kawazoe, Y. *Phys. Rev. B* **2001**, *64*, 233405.
(14) Hunter, J. M.; Fye, J. L.; Jarrold, M. F. *Phys. Rev. Lett.* **1994**, *73*, 2063.
(15) Tai, Y.; Murakami, J.; Majumder, C.; Kumar, V.; Mizuseki, H.; Kawazoe, Y. *Eur. Phys. J. D* **2003**, *24*, 295.
(16) Cheshnovsky, O.; Yang, S. H.; Pettiette, C. L.; Craycraft, M. J.; Liu, Y.; Smally, R. E. *Chem. Phys. Lett.* **1987**, *138*, 119.
(17) Burton, G. R.; Arnold, C. C.; Xu, C.; Neumark, D. M. *J. Chem. Phys.* **1996**, *104*, 2757.
(18) Ganteför, G.; Gausa, M.; Meiwes-Broer, K. H.; Lutz, H. O. *Z. Phys. D: At., Mol. Clusters* **1989**, *12*, 405.
(19) Moravec, V. D.; Klopcic, S. A.; Jarrold, C. C. *J. Chem. Phys.* **1999**, *110*, 5079.
(20) (a) Kawamata, H.; Negishi, Y.; Kishi, R.; Iwata, S.; Nakajima, A.; Kaya, K. *J. Chem. Phys.* **1996**, *105*, 5369. (b) Negishi, Y.; Kawamata, H.; Hayase, T.; Gomei, M.; Kishi, R.; Hayakawa, F.; Nakajima, A.; Kaya, K. *Chem. Phys. Lett.* **1997**, *269*, 199. (c) Negishi, Y.; Kawamata, H.; Nakajima, A.; Kaya, K. *J. Electron Spectrosc.* **2000**, *106*, 117.
(21) Binggeli, N.; Chelikowsky, J. R. *Phys. Rev. Lett.* **1995**, *75*, 493.
(22) Li, S. D.; Zhao, Z. G.; Wu, H. S.; Jin, Z. H. *J. Chem. Phys.* **2001**, *115*, 9255.
(23) Öğüt, S.; Chelikowsky, J. R. *Phys. Rev. B* **1997**, *55*, R4914.
(24) Archibong, E. F.; St-Amant, A. *J. Chem. Phys.* **1998**, *109*, 962.
(25) Gallo, C. F.; Chandrasekhar, B. S.; Sutter, P. H. *J. Appl. Phys.* **1963**, *34*, 144.
(26) Vossloh, C.; Holdenried, M.; Micklitz, H. *Phys. Rev. B* **1998**, *58*, 12422.
(27) Haro-Poniatowski, E.; Serna, R.; Suarez-Garcia, A.; Afonso, C. N.; Jouanne, M.; Morhange, J. F. *Appl. Phys. A* **2004**, *79*, 1299.
(28) Hicks, L. D.; Dresselhaus, M. S. *Phys. Rev. B* **1993**, *47*, 12727.
(29) Dresselhaus, M. S.; Dresselhaus, G.; Sun, X.; Zhang, Z.; Cronin, S. B.; Koga, T. *Phys. Solid State* **1999**, *41*, 679.
(30) Hicks, L. D.; Dresselhaus, M. S. *Phys. Rev. B* **1993**, *47*, 16631.
(31) Thonhauser, T.; Scheidemantel, T. J.; Sofo, J. O. *Appl. Phys. Lett.* **2004**, *85*, 588.
(32) Abeles, B.; Meiboom, S. *Phys. Rev.* **1956**, *101*, 544.
(33) Bate, R. T.; Einspruch, N. C.; May, P. J. *Phys. Rev.* **1969**, *186*, 599.
(34) Uher, C. *J. Phys. F*: *Met. Phys.* **1979**, *9*, 2399.
(35) Boxus, J.; Heremans, J.; Michenaud, J. P.; Issi, J. P. *J. Phys. F*: *Met. Phys.* **1979**, *9*, 2387.
(36) Noh, H. P.; Park, C.; Jeon, D.; Cho, K.; Hashizume, T.; Kuk, Y.; Sakurai, T. *J. Vac. Sci. Technol. B* **1994**, *12*, 2097.
(37) Tang, S. P.; Freeman, A. J. *Phys. Rev. B* **1994**, *50*, 1701.
(38) Serna, R.; Missana, T.; Afonso, C. N.; Ballesteros, J. M.; Petford-Long, A. K.; Doole, R. C. *Appl. Phys. A* **1998**, *66*, 43.
(39) Schmidt, T.; Falta, J.; Materlik, G.; Zeysing, J.; Falkenberg, G.; Johnson, R. L. *Appl. Phys. Lett.* **1999**, *74*, 1391.
(40) Meloni, G.; Gingerich, K. A. *J. Chem. Phys.* **2002**, *116*, 6957.
(41) Maruyama, S.; Anderson, L. R.; Smalley, R. E. *Rev. Sci. Instrum.* **1990**, *61*, 3686.
(42) Mamyrin, B. A.; Shmikk, D. V. *Sov. Phys. JETP* **1979**, *49*, 762.
(43) Xing, X. P.; Tian, Z. X.; Liu, P.; Gao, Z.; Zhu, Q. H.; Tang, Z. C. *Chinese J. Chem. Phys.* **2002**, *15*, 83.
(44) (a) Hay, P. J.; Wadt, W. R. *J. Chem. Phys.* **1985**, *82*, 284. (b) Hay, P. J.; Wadt, W. R. *J. Chem. Phys.* **1985**, *82*, 299.
(45) Check, C. E.; Faust, T. O.; Bailey, J. M.; Wright, B. J.; Gilbert, T. M.; Sunderlin, L. S. *J. Phys. Chem. A* **2001**, *105*, 8111.
(46) Li, G. L.; Xing, X. P.; Tang, Z. C. *J. Chem. Phys.* **2003**, *118*, 6884.
(47) Li, X.; Zhang, H. F.; Wang, L. S.; Kuznetsov, A. E.; Cannon, N. A.; Boldyrev, A. I. *Angew. Chem., Int. Ed.* **2001**, *40*, 1867.
(48) Frisch, M. J.; Trucks, G. W.; Schlegel, H. B.; Scuseria, G. E.; Robb, M. A.; Cheeseman, J. R.; Zakrzewski, V. G.; Montgomery, J. A.; Stratmann, R. E., Jr.; Burant, J. C.; Dapprich, S.; Millam, J. M.; Daniels, A. D.; Kudin, K. N.; Strain, M. C.; Farkas, O.; Tomasi, J.; Barone, V.; Cossi, M.; Cammi, R.; Mennucci, B.; Pomelli, C.; Adamo, C.; Clifford, S.; Ochterski, J.; Petersson, G. A.; Ayala, P. Y.; Cui, Q.; Morokuma, K.; Malick, D. K.; Rabuck, A. D.; Raghavachari, K.; Foresman, J. B.; Cioslowski, J.; Ortiz, J. V.; Baboul, A. G.; Stefanov, B. B.; Liu, G.; Liashenko, A.; Piskorz, P.; Komaromi, I.; Gomperts, R.; Martin, R. L.; Fox, D. J.; Keith, T.; Al-Laham, M. A.; Peng, C. Y.; Nanayakkara, A.; Challacombe, M.; Gill, P. M. W.; Johnson, B.; Chen, W.; Wong, M. W.; Andres, J. L.; Gonzalez, C.; Head-Gordon, M.; Replogle, E. S.; Pople, J. A. *Gaussian 98*; Gaussian, Inc.: Pittsburgh, PA, 1998.
(49) Li, S. D.; Zhao, Z. G.; Zhao, X. F.; Wu, H. S.; Jin, Z. H. *Phys. Rev. B* **2001**, *64*, 195312.
(50) Li, J.; Li, X.; Zhai, H. J.; Wang, L. S. *Science* **2003**, *299*, 864.
(51) Kawamura, H.; Kumar, V.; Kawazoe, Y. *Phys. Rev. B* **2004**, *70*, 245433.
(52) Lau, K. C.; Deshpande, M.; Pandey, R. *Int. J. Quantum Chem.* **2005**, *102*, 656.
(53) Wang, B. L.; Zhao, J. J.; Chen, X. S.; Shi, D. N.; Wang, G. H. *Phys. Rev. A* **2005**, *71*, 33201.
(54) Wang, J. L.; Wang, G. H.; Zhao, J. J. *J. Phys.*: *Condens. Matter* **2001**, *13*, L753.
(55) Hiura, H.; Miyazaki, T.; Kanayama, T. *Phys. Rev. Lett.* **2001**, *86*, 1733.
(56) Zheng, W.; Nilles, J. M.; Radisic, D.; Bowen, K. H. *J. Chem. Phys.* **2005**, *122*, 71101.
(57) Ohara, M.; Koyasu, K.; Nakajima, A.; Kaya, K. *Chem. Phys. Lett.* **2003**, *371*, 490.
(58) Ohara, M.; Miyajima, K.; Pramann, A.; Nakajima, A.; Kaya, K. *J. Phys. Chem. A* **2002**, *106*, 3702.
(59) Lu, J.; Nagase, S. *Phys. Rev. Lett.* **2003**, *90*, 115506.
(60) Sen, P.; Mitas, L. *Phys. Rev. B* **2003**, *68*, 155404.
(61) Khanna, S. N.; Rao, B. K.; Jena, P. *Phys. Rev. Lett.* **2002**, *89*, 16803.
(62) Kawamura, H.; Kumar, V.; Kawazoe, Y. *Phys. Rev. B* **2005**, *71*, 75423.